

# Magnetic properties of Pd atomic clusters from different theoretical approaches

F. Aguilera-Granja<sup>1,a</sup>, A. Vega<sup>1</sup>, J. Rogan<sup>2</sup>, W. Orellana<sup>2</sup>, and G. García<sup>3</sup>

<sup>1</sup> Departamento de Física Teórica, Atómica, y Óptica, Universidad de Valladolid, 47011 Valladolid, Spain

<sup>2</sup> Departamento de Física, Facultad de Ciencias, Universidad de Chile, Casilla 653, Santiago 1, Chile

<sup>3</sup> Facultad de Física, Pontificia Universidad Católica de Chile, Casilla 306, Santiago 7820436, Chile

Received 29 December 2006 / Received in final form 9 April 2007

Published online (Inserted Later) – © EDP Sciences, Società Italiana di Fisica, Springer-Verlag 2007

**Abstract.** We report a comparative study of the magnetic properties of free-standing  $\text{Pd}_N$  clusters ( $2 \leq N \leq 21$ ) obtained through two different theoretical approaches that are extensively employed in electronic structure calculations: a semi-empirical Tight-Binding (TB) model and an ab-initio DFT pseudopotential model. Conclusions are drawn about the reliability of the TB model for the investigation of the electronic structure and magnetic properties of such complex  $4d$  Transition Metals (TM) systems and we compare the results with previous systematic DFT calculations and comment on some available experiments in the literature.

**PACS.** 75.75.+a Magnetic properties of nanostructures – 36.40.Cg Electronic and magnetic properties of clusters – 75.50.-y Studies of specific magnetic materials

## 1 Introduction

Successful production of nanometer scale devices requires a clear understanding of the physical and electronic properties of the system at the atomic level. Since clusters have a wide range of applications, there is a considerable interest in the understanding of their geometrical and electronic structures. The possible existence of ferromagnetism in Pd clusters has been investigated both theoretically and experimentally without finding the last answer due to the complex behavior of this  $4d$  element under low dimensional conditions. Theoretical calculations using semi-empirical and first-principles methods predict, in general, weak ferromagnetic behavior for relatively small size clusters ( $N \leq 55$ ) [1–8], although very recent calculations by Moseler et al. [9] and Kumar et al. [10] obtained relatively high magnetic moments for the  $\text{Pd}_{13}$  cluster in the framework of the density functional theory (DFT) using pseudopotentials and the GGA approximation for the exchange and correlation potential, being this magnetic moment higher than the experimental estimate. From the experimental side, most of the studies have found either non-magnetic behavior or very weak magnetic moments [11–14] and only very recently large magnetization at the surface of fine Pd particles ( $0.75 \pm 0.31 \mu_B$  per atom) was reported [15] (in contrast with a previous work of the same group [14] that reported very weak surface magnetic moment of  $0.23 \pm 0.19 \mu_B$  per atom). All these

results give further support to the complex behavior of the Pd clusters.

From the theoretical point of view, the DFT methods and the TB models are the two most extensively used approaches. Considering the width dispersion in the results, and with the aim to shed some light in this complex scenario, it is worth performing a benchmark between both approaches and in particular to analyze the reliability of the TB model, which being considered as less accurate than DFT, however it requires a much less computational efforts (memory and CPU time) than the DFT methods.

For our purpose, we have performed a systematic study of the electronic structure and magnetic properties for  $\text{Pd}_N$  ( $2 \leq N \leq 21$ ) clusters using on the one hand, the ab-initio pseudopotential DFT method, as implemented in the SIESTA code, and on the other hand a self-consistent real space *spd* TB method. In particular, we calculate the magnetic moment as a function of the cluster size. As a first step, the geometrical structures are determined using a Genetic Algorithm (GA) on a phenomenological Gupta potential, and then re-optimized with conjugate gradients as implemented in the SIESTA code. The electronic properties of those structures are studied using both SIESTA and TB and compared. We will also discuss our results in the context of systematic DFT calculations available in the literature [10, 16].

The paper is organized as follows, in Section 2 we briefly present the theoretical models. In Section 3, our results are discussed and compared with previous works, and Section 4 summarizes the main conclusions.

<sup>a</sup> e-mail: faustino@dec1.ifisica.uaslp.mx

## 2 Computational methods

### 2.1 Genetic algorithm

In order to determine the minimum energy cluster structure we use a genetic algorithm, which is a global search technique based on the principles of natural evolution [17–20].

In particular, we implemented a steady-state GA that uses a combination of the coordinates of each atom, as our genome, and applies an additional local minimizer (classical simplex and Monte Carlo) within the basin [21]. This combination considerably improves the convergence speed, and has proven to be quite reliable [21, 22]. As it is standard in a steady-state GA, we chose the parents by the roulette wheel selection method, and we specify the fraction of the population that remains unchanged (elitism). To produce a new generation we adopt the genetic operators described by Niesse and Mayne [21].

For a fixed number  $N$  of atoms in the cluster, we performed computations for ten different populations (each of them with 30 individuals). The initial atomic positions were chosen at random, while the elitism percentage adopted was 30%. For  $N = 2$ –13, we used 5000 iterations but for  $N = 14$ –21, 10 000 iteration were needed to converge to the minimum.

The energy in the GA was computed with the Gupta phenomenological potential [23, 24] which was derived from Gupta's expression for the cohesive energy of a bulk material [23] and is based on the second moment approximation to the tight binding theory. It is a potential that has a very simple analytical form, depending only on five parameters. The explicit functional form for the cohesive energy and the parameter values for Pd used in our calculations are given by Cleri and Rosato [24]. The parameters of the potential are fitted to bulk properties: cohesive energy, lattice parameter, independent elastic constants, and the vanishing of the energy gradient at the equilibrium distance.

### 2.2 Ab-initio DFT pseudopotential calculations

We have performed first-principles DFT calculations using the pseudopotential SIESTA code (Spanish Initiative for Electronic Simulation of Thousand Atoms) [25]. This method employs linear combination of pseudoatomic orbitals as basic sets. The atomic core is replaced by a non-local norm-conserving Troullier-Martins [26] pseudopotential that is factorized in the Kleinman-Bilander form [27] and may include nonlinear terms correcting for the significant overlap of the core charges with the valence  $d$  orbitals.

To optimize the geometrical structures we did a local relaxation using the conjugate gradient algorithm, starting from the structures obtained via the genetic algorithm search on a Gupta potential.

In the present calculation, we have used for the exchange and correlation potential the LDA as parametrized by Perdew-Zunger [28]. We have recently demonstrated that within the SIESTA code, the ground state of small

Pd clusters (up to 7 atoms) does not depend upon the choice of LDA or GGA for the exchange and correlation potential [29]. The ionic pseudopotentials were generated using the atomic configurations:  $4d^9$ ,  $5s^1$  and  $5p^0$  for Pd with 2.0, 2.2 and 2.4 a.u. cutoff radii, respectively. The core corrections are included with a radius of 1.2 a.u. We have found from the various pseudopotentials tested that the  $4d^9$ ,  $5s^1$  configuration reproduced slightly better the eigenvalues of different excited states of the isolated Pd atom than the  $4d^{10}$ ,  $5s^0$  configuration. Besides, the ab-initio electronic occupations of small Pd clusters are closer to this configuration [29] than to the  $4d^{10}$ ,  $5s^0$ . Valence states have been described using DZP basis sets with two orbitals having different radial form to describe both the  $5s$  and the  $4d$  shells of Pd and one orbital to describe the  $5p$  shell. We consider an electronic temperature of 25 meV and a 120 Ry energy cutoff has been used to define the real space grid for numerical calculations involving the electron density, a larger cutoff does not substantially modify the results.

### 2.3 Semiempirical real-space tight-binding calculations

The spin-polarized electronic structure was determined by solving self-consistently a TB Hamiltonian for the  $4d$ ,  $5s$  and  $5p$  valence electrons in a mean-field approximation. The Hamiltonian can be expressed as follows;

$$H = \sum_{i\alpha\sigma} \varepsilon_{i\alpha\sigma} \hat{n}_{i\alpha\sigma} + \sum_{\substack{\alpha\beta\sigma \\ i \neq j}} t_{ij}^{\alpha\beta} \hat{c}_{i\alpha\sigma}^\dagger \hat{c}_{j\beta\sigma}, \quad (1)$$

where  $\hat{c}_{i\alpha\sigma}^\dagger$  is the operator for the creation of an electron with spin  $\sigma$  and orbital state  $\alpha$  at the atomic site  $i$ ,  $\hat{c}_{j\beta\sigma}$  is the annihilation operator and  $\hat{n}_{i\alpha\sigma}$  is the number operator.

The hopping integrals  $t_{ij}^{\alpha\beta}$  between orbitals  $\alpha$  and  $\beta$  at sites  $i$  and  $j$  describe the electronic de-localization within the system, which is relevant for itinerant magnetism. In this work, we considered hopping integrals up to third nearest neighbor distances. These integrals are assumed to be spin-independent and have been fitted to reproduce the band structure of bulk Pd [30]. However, since interatomic distances in the clusters differ slightly from the bulk, the variation of hopping integrals with the interatomic distance  $r_{ij}$  has been explicitly considered using the typical power law  $(r_0/r_{ij})^{l+l'+1}$ , where  $r_0$  is the bulk equilibrium distance and  $l, l'$  are the orbital angular momenta of the  $(i\alpha\sigma)$  and  $(j\beta\sigma)$  states involved in the hopping process [31].

The spin-dependent diagonal terms account for the electron-electron interaction through a correction shift of the energy levels

$$\varepsilon_{i\alpha\sigma} = \varepsilon_{i\alpha}^0 + z_\sigma \sum_{\beta} \frac{J_{\alpha\beta}}{2} \mu_{i\beta} + \Omega_{i\alpha}. \quad (2)$$

Here,  $\varepsilon_{i\alpha}^0$  are the bare orbital energies of paramagnetic bulk Pd. The second term is the correction shift due to the

**Table 1.** The cluster size ( $N$ ), the symmetry (structure), the average interatomic distance in Å (distance), average coordination number ( $Z$ ) and the magnetic moment from the Tight-Binding (TB), SIESTA, Futschek and Kumar calculations, respectively. Those values marked with a label in parenthesis correspond to an Isomer within Futschek’s calculation [16]. (a) Isomer at 10 meV from their double trigonal antiprism ground state, (b) isomer at 17 meV from their edge sharing octahedral-like ground state, (c) isomer at 20 meV from their edge sharing octahedral-like ground state. Absent values in the last two columns correspond to those clusters for which Futschek et al. and Kumar et al. do not report isomers with the geometry of the second column.

$N$	structure	distance	$Z$	TB	SIESTA	Futschek	Kumar
2	dumbbell	2.45	2.00	0.98	1.00	1.00	1.00
3	triangle	2.50	2.00	0.00	0.66	0.00	0.66
4	tetrahedron	2.58	3.00	0.48	0.50	0.50	0.50
5	trigonal bipyramid	2.62	3.60	0.38	0.40	0.40	0.40
6	octahedron (O)	2.63	4.00	0.35	0.33	0.33	0.00
7	pentagonal bipyramid (PB)	2.66	4.60	0.61	0.29	0.29	0.29
8	O+2	2.64	4.50	0.50	0.49	0.25	0.25
9	PB+2	2.67	5.12	0.49	0.44	0.44 (a)	0.44
10	PB+3	2.68	5.40	0.59	0.60		0.60
11	PB+4	2.69	5.64	0.36	0.55		0.55
12	PB+5	2.70	6.00	0.49	0.50	0.50 (b)	0.50
13	icosahedron (I)	2.71	6.50	0.61	0.62	0.62 (c)	0.62
14	I+1	2.68	6.43	0.13	0.57		0.57
15	I+2	2.68	6.53	0.12	0.53		0.53
16	distorted I-like	2.68	6.38	0.00	0.25		
17	distorted I-like	2.67	6.67	0.04	0.24		
18	distorted I-like	2.67	6.44	0.05	0.34		
19	double Icosahedron (DI)	2.69	7.16	0.41	0.32		0.32
20	distorted DI	2.68	6.70	0.10	0.30		
21	distorted DI	2.70	7.05	0.15	0.29		

spin-polarization of the electrons at site  $i$  ( $\mu_{i\beta} = \langle n_{i\beta\uparrow} \rangle - \langle n_{i\beta\downarrow} \rangle$ ).  $J_{\alpha\beta}$  are the exchange integrals and  $z_{\sigma}$  is the sign function ( $z_{\uparrow} = 1$ ,  $z_{\downarrow} = -1$ ).

As usual, the exchange integrals involving  $s$  and  $p$  electrons were neglected taking into account only the integral corresponding to  $d$  electrons ( $J_{dd}$ ). Note that although the  $sp$  exchange integrals are neglected, spin-polarization of the de-localized  $sp$  states will exist as a consequence of hybridization with the  $d$  states. Usually  $J_{dd}$  is obtained by fitting to the bulk magnetic moment. However, since palladium bulk metal is paramagnetic, the exchange parameter ( $J_{dd} = 0.60$  eV) has been chosen such that reproduces the ab-initio DFT calculations of the average magnetic moment of a Pd<sub>13</sub> icosahedral cluster by Moseler et al. [9] and Kumar et al. [10] We have chosen the Pd<sub>13</sub> cluster for the fit because it is the most studied cluster in the literature, and agreement exists concerning its icosahedral geometry.

The site- and orbital-dependent self-consistent potential  $\Omega_{i\alpha}$  assures the local electronic occupation, fixed in our model by linearly interpolating between the atom and the metal occupations according to the local coordination at site  $i$ . We have used [Kr]  $4d^9 5s^1$  for the electronic configuration of Pd atom. The metal electronic occupations, on the other hand, are 0.60, 0.45, and 8.95 for the  $s$ ,  $p$ , and  $d$  electrons of Pd, respectively. The local neutrality approximation used in this work has been probed to be a good approximation in transition metal systems [32] and in the present case, atomic and bulk  $sp$  and  $d$  occupations are similar.

The spin-dependent local electronic occupations are self-consistently determined from the local densities of states

$$\langle \hat{n}_{i\alpha\sigma} \rangle = \int_{-\infty}^{\varepsilon_F} \mathcal{D}_{i\alpha\sigma}(\varepsilon) d\varepsilon, \quad (3)$$

which are calculated at each iteration by using the recursion method [31]. In this way, the distribution of the local magnetic moments ( $\mu_i = \sum_{\alpha} \mu_{i\alpha}$ ) and the average magnetic moment per atom ( $\bar{\mu} = \frac{1}{N} \sum_i \mu_i$ ) of the Pd <sub>$N$</sub>  clusters are obtained at the end of the self-consistent cycle. The number of recursion levels used in our calculation is large enough to assure the stability of the results. The imaginary part of the energy for the calculation of the density of states within the recursion method is chosen so as to correspond to the electronic temperature used in SIESTA.

The same model was used in previous works [33] for the study of Rh clusters and for the study of the single FCC-like Pd clusters [34]. The good agreement with available data in the literature for free clusters, give us confidence in the transferability of the parameterization.

### 3 Geometrical structures

In Table 1, we list the main geometrical and electronic properties of the palladium clusters [35], illustrated in Figure 1. In general, we obtain an icosahedral-like growth pattern with some structural disorder, particularly between symmetric closed shell clusters ( $N = 8$  to 13, 13

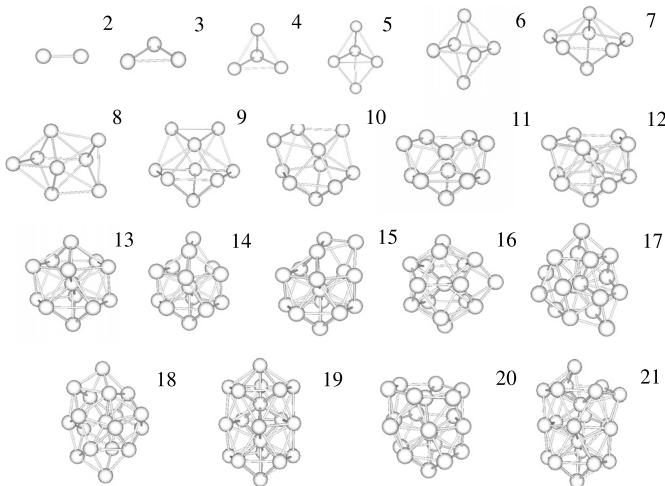


**Fig. 1.** Ground-state geometric structures of  $\text{Pd}_N$  clusters ( $2 \leq N \leq 21$ ) obtained with the SIESTA code.

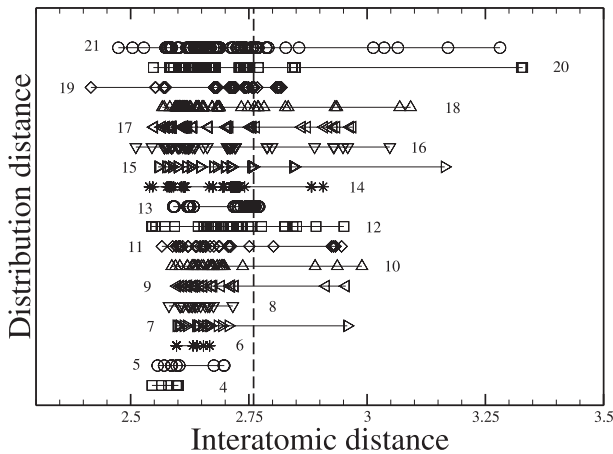


**Fig. 2.** Distribution of the first nearest neighbours distance (in Å) within the different clusters ( $N = 4$  to 21). The numbers correspond to the cluster size  $N$ , the horizontal lines quantify the dispersion of the interatomic distances, and the vertical dashed line marks the fcc Pd bulk interatomic distance.

to 19) and for  $N = 20$  and 21. To illustrate such structural disorder within the clusters, we plot in Figure 2 the distribution of first nearest neighbour (FNN) distances. At a given site  $i$  within the cluster, we consider as FNN those atoms located at distances within 0.85 to 1.15 of the bulk interatomic one. The structural disorder in our clusters (reflected by the absence of a discrete number of well defined interatomic distances) results from the fully unconstrained relaxation process. Slightly non-symmetrical arrangements are obtained for the closed shell clusters. Notice that the structural disorder or amorphization is more pronounced for the open shell clusters. For the closed shell ones (see for instance  $N = 13$  and  $N = 19$ ) there are two and three well defined interatomic distances, respectively.

Let us now compare these geometric structures with those obtained by Futschek et al. [16], using the VASP DFT code in the GGA approximation and by Kumar et al. [10] using an ultra-soft pseudopotentials DFT GGA method. In comparison with Futschek et al. [16], for clusters with  $N \leq 8$  the geometries are essentially the same, whereas for larger clusters they are different. For  $N = 9$  to 13 Futschek et al. predict double trigonal antiprism ( $N = 9$ ) and edge sharing octahedral plus additional atoms ( $N = 10$  to 13). In contrast we predict for  $N = 9$  to 13 pentagonal bipyramids of seven atoms plus additional atoms building the icosahedral shape.

As a summary, in the case of  $N \leq 13$ , Futschek's Pd clusters can be seen as relaxed fragments of the fcc crystal bulk structure, whereas ours are mainly non-crystalline structures, particularly in the range of  $7 \leq N \leq 13$ , in which five fold symmetry is observed.

Comparing with Kumar et al., for  $N = 2$ –15 and 19, their geometries are similar as ours. For the rest of the clusters their structures are icosahedral-like. In our case, for  $N = 16$ –18, 20 and 21, the structures have some structural disorder as previously described in Figure 2. Otherwise they are also icosahedral-like.

In general, clusters having similar structures have also similar interatomic distances (within 2%) in both our SIESTA calculations and in Futschek et al. and Kumar et al. calculations.

But It is important to stress that differences in the geometrical structures are obtained in some clusters, as indicated above, depending on the approximations used for the exchange-correlation potential and for the treatment of the core states within the DFT.

## 4 Magnetic moments

The spin magnetic moment is obtained from the difference between the electronic populations with different spin component. Therefore for its determination it is not crucial to exactly determine the position of the electronic states as long as the occupied states are well counted. In Figure 3 we present the average magnetic moment per atom for the ground state Pd clusters, as calculated with TB and SIESTA. For the sake of comparison, we have also included the ground state results by Kumar et al. [10] and by Futschek et al. [16] when available. In general the TB and the SIESTA magnetic trends as increasing cluster size are in a fairly good agreement, similar to the one existing between SIESTA and other DFT calculations. This is illustrated also in Table 1, where we show the results for those sizes for which the same geometry can be obtained from the three DFT calculations (notice that for  $N = 9$  to 13, the geometries considered from Futschek et al. are metastable isomers).

Let us enter now in more detail. When we compare our SIESTA and TB calculations, we can distinguish two regions as far as the magnetic behavior is concerned. For clusters with  $N \leq 13$ , the magnetic moments resulting from both calculations are in general very similar (not only the general trend but also the numerical values); the

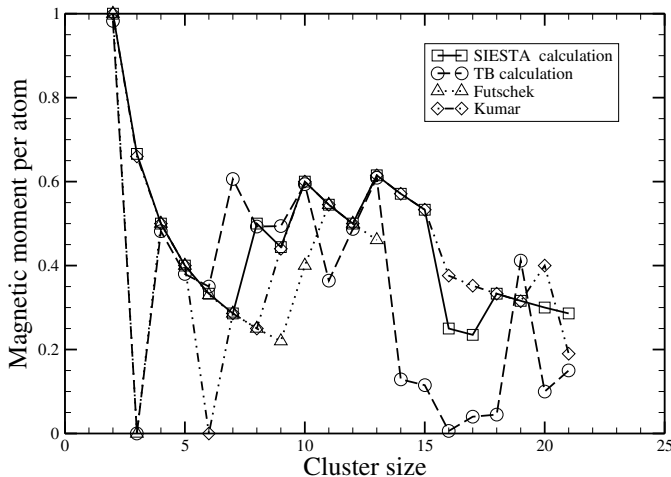


**Fig. 3.** Average magnetic moment per atom as a function of the cluster size obtained from SIESTA and TB calculations. We also report the results of references [10,30].

differences are located at  $N = 3, 7$ , and  $11$ . The largest difference corresponds to  $N = 3$ , for which the TB calculation predicts a non-magnetic behavior whereas the SIESTA calculation gives a magnetic solution. However, it is worth noticing that in Futschek’s DFT calculation, both solutions are degenerated and may coexist. For  $N \geq 14$ , the TB calculation underestimate in general the magnetic moment (an exception being  $N = 19$ ) although both calculations lead to a similar trend, with minima around  $N = 16$  and  $17$ . Notice that these minima are not found in the DFT calculations of Kumar et al. that, on the other hand, overestimate the SIESTA results.

Pursuing the comparison among the different DFT results, for  $N = 2, 4-7$ , our SIESTA calculation gives the same magnetic moments as Futschek et al. [16]. For  $N = 6$  we have a magnetic octahedron as the ground state whereas Kumar et al. [10] has a non-magnetic solution. However Kumar’s magnetic solution is only 3 meV per atom above the non-magnetic one [29] (nearly degenerated). For  $\text{Pd}_8$ , our magnetic moment is different to that found in other DFT calculations, despite having the same ground-state structure. Our most stable solution has  $0.50 \mu_B$  per atom whereas Futschek et al. and Kumar et al. obtain  $0.25 \mu_B$  per atom. It is worth noticing that Futschek et al. have found another metastable magnetic solution with  $0.50 \mu_B$  per atom for the same geometrical structure, with an energy difference of 11 meV per atom. For  $\text{Pd}_9$  Futschek et al. predict a double trigonal antiprism with  $0.22 \mu_B$  per atom whereas we obtain a pentagonal bipyramid plus two additional atoms, with a magnetic moment per atom of  $0.44 \mu_B$ . For this size, our calculation agrees with Kumar’s result both in the structure and in the magnetic moment. In the case of  $\text{Pd}_{10}$ , the structure and the total magnetic moment obtained by us and by Futschek et al. are very different. Our structure is icosahedral-like and the magnetic moment per atom is  $0.60 \mu_B$  whereas Futschek’s structure is an edge sharing

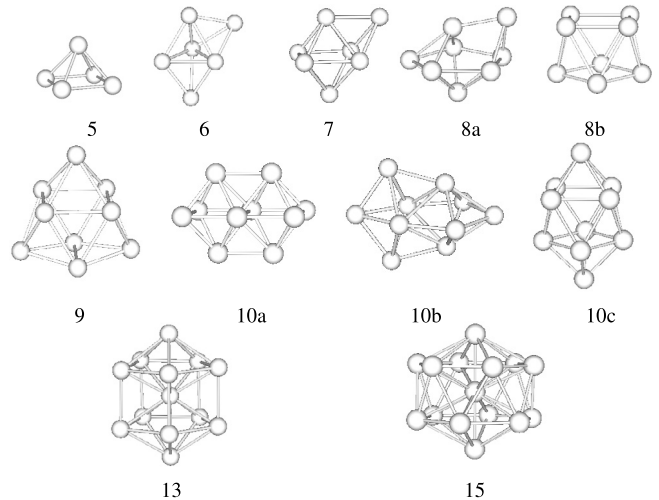


**Fig. 4.** Geometric structures of some selected isomers of  $\text{Pd}_N$  ( $5 \leq N \leq 15$ ) in an increasing order of their size and energy.

double octahedra and the magnetic moment is  $0.40 \mu_B$ . For  $N = 11$  and  $12$ , our results agree with those of Kumar and with one of the isomers given in Futschek’s work. Finally, for  $N = 13$ , our lower energy structure is icosahedral with a magnetic moment of  $0.61 \mu_B$ , which is the same structure found by Kumar et al. [10]. Futschek’s ground state structure is an edge sharing octahedral plus three additional atoms, with magnetic moment of  $0.46 \mu_B$ ; the corresponding icosahedron calculated by Futschek et al. is 10 meV per atom above their ground state and with the same magnetic moment as our SIESTA value.

In general our geometric structures and magnetic moments are in better agreement with those of Kumar’s et al. than with those of Futschek et al., and differences exist among the different DFT calculations.

The overall results are consistent with the experiments that find weak magnetic moments [11–14]. In particular, Cox’s experimental observations indicate that  $\text{Pd}_{13}$  has a magnetic moment of  $\approx 0.4 \mu_B$  per atom. A decrease in the magnetic moment with the cluster size is also found [11,12]. No further comparison is possible due either to the lack of detailed results in the small size region or to the huge cluster sizes grown in some experimental studies [13,14].

With the aim to see the dependence of the magnetic moment with the different structures in a more systematic way, we have calculated the average magnetic moment of some selected isomers and compared the results with those obtained for the ground state as calculated with SIESTA. The isomers are illustrated in Figure 4 and the corresponding structural data and energy difference with respect to the ground state are summarized in Table 2. For certain sizes, we have considered several isomers because their highly symmetric closed shell geometric structure or because they correspond to the ground state or to the first isomer reported in other DFT calculations [10,16]. For instance, in the case of  $N = 8$ , the structures shown in Figure 4 have been reported by Kumar and cowork-

**Table 2.** We give, for the isomers illustrated in Figure 4, structure, the average interatomic distance, average coordination number ( $Z$ ), average magnetic moment (AMM), and energy difference per atom with respect to the ground state calculated with the SIESTA.

$N$	structure	distance	$Z$	AMM	$\Delta E$ (meV)
5	square pyramid	2.58	3.20	0.40	4
6	trigonal bipyramid + 1	2.65	4.00	0.33	64
7	O + 1	2.64	4.28	0.28	18
8a	PB + 1	2.66	4.75	0.50	34
8b	tetragonal antiprism	2.62	4.00	0.00	39
9	tricapped prism	2.64	4.66	0.44	24
10a	double O	2.65	5.00	0.40	4
10b	two interlinked PB	2.67	5.20	0.40	22
10c	tetragonal antiprism + 2	2.64	4.80	0.40	43
13	decahedron	2.68	5.69	0.62	35
15	hexagonal antiprism+2	2.73	6.66	0.40	12

ers [10], whereas the ground state in our case is the O+2 structure (octahedron plus two atoms or dodecahedron as illustrated in Fig. 1). In the case of  $N = 10$ , we have calculated the magnetic moment of three different isomers, the first one (10a) has been reported as the ground state by Futschek and coworkers [16] whereas the other two (10b and 10c) are closer isomers obtained by Kumar and coworkers [10].

The average interatomic distances for the different isomers are within less than 2% with respect to the ground state (see Tabs. 1 and 2). For several isomers, we have found energy differences of the order of few meV/atom, indicating a possible coexistence of those isomers with the ground state at room temperature, however for this analysis it would require a thorough study in which the vibrational modes should be calculated for the determination of the entropy and free energy necessary for obtaining the relative population of the different isomers [33]. The study itself is interesting but is cumbersome and is not our intention to perform this work inhere. Moreover, in general the average magnetic moments of these isomer are similar to those obtained for the ground state, with only some exceptions like the tetragonal antiprism (second cluster shown for  $N = 8$ ) whose average magnetic moment is  $0 \mu_B$  and for  $N = 10$  for which the three isomers have an average magnetic moment of  $0.4 \mu_B$  instead of  $0.6 \mu_B$  obtained for the corresponding ground state (PB+3). Differences with the values reported by other calculations are also exceptional.

## 5 Conclusions

We have performed a systematic study of the magnetic moments of  $\text{Pd}_N$  ( $2 \leq N \leq 21$ ) clusters using the ab-initio pseudopotential DFT method, as implemented in the SIESTA code, and a self-consistent real space *spd* TB method, in order to perform a benchmark of two of the most extensively used approaches in this field.

The TB and the SIESTA results are in a fairly good qualitative agreement, similar to the agreement between SIESTA and other DFT calculations. The overall results for the magnetic properties are consistent with the experiments that find weak magnetic moments in Pd clusters [11–14].

We acknowledge the financial support from PROMEP-SEP-CA230, CONACyT 2005–50650, Junta de Castilla y León at Spain (project VA068A06), spanish Ministry of Education and Science (project MAT2005-03415 and SAB2004-0129) in conjunction with the European Regional Development Fund, *Fondo Nacional de Investigaciones Científicas y Tecnológicas* of Chile (grant 1070080 and 1071062 (J.R.)) and the Millennium Nucleus of Applied Quantum Mechanics and Computational Chemistry (project P02-004-F(W.O.)). We also acknowledge to J. Limón-Castillo for the help in some computational details.

## References

1. B.V. Reddy, S.N. Khanna, B.I. Dunlap, *Phys. Rev. Lett.* **70**, 3323 (1993)
2. F. Salcido-Ayala, P. Villaseñor-González, J.G. Dorantes-Dávila, *Rev. Mex. Fís.* **45**, 443 (1998)
3. S. Bouarab, C. Demangeat, A. Mokrani, H. Dreyssé, *Phys. Lett. A* **151**, 103 (1990)
4. J.P. Bucher, L.A. Bloomfield, *Int. J. Mod. Phys. B* **7**, 1079 (1993)
5. K. Lee, *Phys. Rev. B* **58**, 2391 (1998)
6. C. Barretau, R. Guirado-López, D. Spanjaard, M.C. Desjonquères, *Phys. Rev. B* **61**, 7781 (2000)
7. L. Vitos, B. Johansson, J. Kollár, *Phys. Rev. B* **62**, R11954 (2000)
8. G.W. Zhang, Y.P. Feng, C.K. Ong, *Phys. Rev. B* **54**, 17208 (1996)
9. M. Moseler, H. Häkkinen, R.N. Barnett, U. Landman, *Phys. Rev. Lett.* **86**, 2545 (2001)
10. V. Kumarn, Y. Kawazoe, *Phys. Rev. B* **66**, 144413 (2002)
11. D.C. Douglass, J.P. Bucher, L.A. Bloomfield, *Phys. Rev. B* **45**, 6341 (1992)
12. A. Cox, J.G. Louderback, S.E. Apsel, L.A. Bloomfield, *Phys. Rev. B* **49**, 12295 (1994)
13. B. Sampedro, P. Crespo, A. Hernando, R. Litrán, J.C. Sánchez-López, C. López-Cartes, A. Fernandez, J. Ramírez, J. González-Calbet, M. Válet, *Phys. Rev. Lett.* **91**, 237203 (2003)
14. T. Taniyama, E. Ohta, T. Sato, *Europhys. Lett.* **38**, 195 (1997)
15. T. Shinohara, T. Sato, T. Taniyama, *Phys. Rev. Lett.* **91**, 197201 (2003)
16. T. Futschek, M. Marsman, J. Hafner, *J. Phys.: Condens. Matter* **17**, 5927 (2005)
17. J. Holland, *Adaptation in Natural and Artificial System*, (University of Michigan Press, Ann Arbor, MI, USA, 1975)
18. D.E. Goldberg, *Genetic Algorithms in Search, Optimizations & Machine Learning* (Addison-Wesley, Reading, MA, USA, 1989)
19. M. Mitchell, *An Introduction to Genetic Algorithms* (MIT Press, Cambridge, MA, USA, 1998)

20. D.M. Deaven, N. Tit, J.R. Morris, K.M. Ho, *Chem. Phys. Lett.* **256**, 195 (1996)
21. J.A. Niese, H.R. Mayne, *J. Chem. Phys.* **105**, 4700 (1996)
22. M. Iwamatsu, *J. Chem. Phys.* **112**, 109760 (2000)
23. R.P. Gupta, *Phys. Rev. B* **23**, 6265 (1985)
24. F. Cleri, V. Rosato, *Phys. Rev. B* **48**, 22 (1993)
25. J.M. Soler, E. Artacho, J.D. Gale, A. García, J. Junquera, P. Ordejon, D. Sánchez-Portal, *J. Phys.: Condens. Matter* **14**, 2745 (2002)
26. N. Troullier, J.L. Martins, *Phys. Rev. B* **43**, 1993 (1991)
27. L. Kleinman, D.M. Bilander, *Phys. Rev. Lett.* **48**, 1425 (1982)
28. J. Perdew, A. Zunger, *Phys. Rev. B* **23**, 5048 (1981)
29. F. Aguilera-Granja, A. Vega, J. Ferrer, *Phys. Rev. B* **74**, 174416 (2006)
30. D.A. Papaconstantopoulos, *Handbook of the Band Structure of Elemental Solids* (Plenum, New York, 1986)
31. R. Haydock, *Solid State Physics*, edited by E. Ehrenreich, F. Seitz, D. Turnbull (Academic Press, London, 1980), Vol. 35, p. 215
32. E. Martínez, R. Robles, A. Vega, R.C. Longo, L.J. Gallego, *Euro. Phys. J. D* **34**, 51 (2005)
33. F. Aguilera-Granja, J.L. Rodríguez-López, K. Michaelian, E.O. Berlanga-Ramírez, A. Vega, *Phys. Rev. B* **66**, 224410 (2002)
34. F. Aguilera-Granja, J.M. Montejano-Carrizales, A. Vega, *Phys. Lett. A* **332**, 107 (2004)
35. J. Rogan, G. García, J.A. Valdivia, W. Orellana, A.H. Romero, R. Ramírez, M. Kiwi, *Phys. Rev. B* **72**, 115421 (2005); J. Rogan, G. García, J.A. Valdivia, W. Orellana, R. Ramírez, M. Kiwi, sent for it publication